# Keck, Gemini, and Palomar 200-inch visible photometry of red and very-red Neptunian Trojans

B. T. Bolin, C. Fremling, A. Morbidelli, K. S. Noll, J. van Roestel, E. K. Deibert, M. Delbo, G. Gimeno, J. -E. Heo, C. M. Lisse, et al.

Monthly Notices of the ROYAL ASTRONOMICAL SOCIETY

MNRAS **521,** L29–L33 (2023) https://doi.org/10.1093/mnrasl/slad018
Advance Access publication 2023 February 14

# Keck, gemini, and palomar 200-inch visible photometry of red and very-red neptunian trojans

B. T. Bolin ,[1,2,3★†] C. Fremling,[2,4] A. Morbidelli,[5,6] K. S. Noll,[1] J. van Roestel,[2,7] E. K. Deibert,[8] M. Delbo,[5] G. Gimeno,[8] J.-E. Heo,[8] C. M. Lisse,[9] T. Seccull[10] and H. Suh[10]

[1]*Goddard Space Flight Center, 8800 Greenbelt Road, Greenbelt, MD 20771, USA*
[2]*Division of Physics, Mathematics and Astronomy, California Institute of Technology, Pasadena, CA 91125, USA*
[3]*Infrared Processing and Analysis Center, California Institute of Technology, Pasadena, CA 91125, USA*
[4]*Caltech Optical Observatories, California Institute of Technology, Pasadena, CA 91125, USA*
[5]*Laboratoire Lagrange, UMR7293, Université de Nice Sophia-Antipolis, CNRS, Observatoire de la Côte d'Azur, F-06300, Nice, France*
[6]*Collège de France, 75231 Paris, France*
[7]*Anton Pannekoek Institute for Astronomy, University of Amsterdam, 1090 GE Amsterdam, The Netherlands*
[8]*Gemini Observatory/NSF's National Optical-Infrared Astronomy Research Laboratory, Casilla 603, La Serena, Chile*
[9]*Johns Hopkins University Applied Physics Laboratory, 11100 Johns Hopkins Rd, Laurel, MD 20723, USA*
[10]*Gemini Observatory/NSF's NOIRLab, 670 N. A'ohoku Place, Hilo, Hawaii, 96720, USA*

Accepted 2023 February 8. Received 2023 February 8; in original form 2023 January 20

## ABSTRACT

Neptunian Trojans (NTs), trans-Neptunian objects in 1:1 mean-motion resonance with Neptune, are generally thought to have been captured from the original trans-Neptunian protoplanetary disc into co-orbital resonance with the ice giant during its outward migration. It is possible, therefore, that the colour distribution of NTs is a constraint on the location of any colour transition zones that may have been present in the disc. In support of this possible test, we obtained *g*, *r*, and *i*-band observations of 18 NTs, more than doubling the sample of NTs with known visible colours to 31 objects. Out of the combined sample, we found ≈4 objects with $g - i$ colours of >1.2 mags placing them in the very red (VR) category as typically defined. We find, without taking observational selection effects into account, that the NT $g - i$ colour distribution is statistically distinct from other trans-Neptunian dynamical classes. The optical colours of Jovian Trojans and NTs are shown to be less similar than previously claimed with additional VR NTs. The presence of VR objects among the NTs may suggest that the location of the red to VR colour transition zone in the protoplanetary disc was interior to 30 – 35 au.

**Key words:** Kuiper Belt: general – minor planets – asteroids: general.

## 1 INTRODUCTION

Understanding how the composition of the Solar system's protoplanetary disc varied as a function of the heliocentric distance has always been a key problem of planetary science with implications on the formation of planetesimals, planets, meteorites, and the delivery of organics, water and pre-biotic materials to planets (Williams & Cieza 2011). While it is now understood that the contemporary asteroid main belt consists of objects that originally accreted in the terrestrial planet and Jupiter formation regions, as well as objects that were implanted from the primordial Kuiper belt (DeMeo & Carry 2014), the compositional structure of the original trans-Neptunian disc (TND) is not yet understood.

It has been theoretically demonstrated that the original configuration of the TND was a low-inclination formation, starting from 23 au with a drop in density past 30 au (Morbidelli & Nesvorný 2020). The TND may have had a colour gradient of trans-Neptunian objects (TNOs) increasing in redness with heliocentric distance due to the sublimation of surface volatiles such as ammonia, methanol, and hydrogen sulfide (Brown et al. 2011; Wong & Brown 2016; Schwamb et al. 2019). The present-day TND consists of the Hot Classical objects (HCs), comprised of bodies that may have formed within 30 au but were scattered outwards by the migration of Neptune, and the Cold Classical objects (CCs), comprised of bodies that probably formed outside of 30 au and had much-reduced interactions with Neptune (Morbidelli & Nesvorný 2020). The resonant population consists of TNOs that are in mean motion resonances with Neptune located at >30 au from the Sun such as the 5:4, 4:3 and 5:3 mean motion resonances at ∼34.7 au, ∼36.2 au, and ∼42.4 au. The ratio p:q denotes the resonance of p orbital periods of Neptune to q periods of the TNO (Gladman, Marsden & Vanlaerhoven 2008). Scattered disc objects are TNOs that are on orbits which are currently scattering off Neptune such that their semimajor axes, *a* change by more than 1.5 au in 10 myr (Morbidelli, Emel'yanenko & Levison 2004). In addition to the HCs, CCs, resonant objects, and scattered disc objects, the Neptunian Trojans (NTs) located at ≈30 au in the Sun-Neptune L4 and L5 Lagrange points (Sheppard & Trujillo 2006), are hypothesized to have been captured from the TND into co-orbital resonances

★ E-mail: bryce.bolin@nasa.gov
† NASA post-doctoral program fellow.

with Neptune during its outward migration (Gomes & Nesvorný 2016).

The colours of TNOs are known to be bimodally distributed between 'red' (R) and 'very-red' (VR) object colours (Hainaut, Boehnhardt & Protopapa 2012) where R objects are defined as having an optical spectral slope of $\lesssim$20 % / 100 nm corresponding to a $g - i$ colour index of $<$1.2 (Sheppard 2012) in the SDSS $g$ and $i$ bandpasses (Fukugita et al. 1996). The 'very-red' (VR) category of TNOs are defined as having an optical spectral slope $\gtrsim$20 % / 100 nm corresponding to a $g - i$ colour index of $>$1.2 (Wong & Brown 2017). The HCs are a more equal mixture of 'red' (R) and 'very-red' (VR) objects while the CCs have a higher ratio in the number of VR objects to the number of R objects (Trujillo & Brown 2002). One of the explanations for the colour dichotomy between R and VR objects is that the original TND had a colour transition boundary from R to VR objects occurring in the primordial disc between $\approx$30 and $\approx$40 au (Nesvorný et al. 2020).

Out of 32 known L4 and L5 Lagrange point NTs (e.g. Sheppard & Trujillo 2006; Parker et al. 2013; Bernardinelli et al. 2022), 16 have optical colours which cover a wide range in optical slope with the majority having an optical spectral slope of $<$20 % / 100 nm or $g - i < 1.2$ (Jewitt 2018). Presently, only one NT is known to have colours that place it in the VR category, 2013 $VX_{30}$ with $g - i = 1.52 \pm 0.06$ Lin et al. (2019). The dearth of VR category objects is surprising because the NTs were captured at a similar heliocentric distance as HCs, but HCs have a higher VR to R colour ratio. This suggests that the transition boundary between R and VR objects was actually much further out from where the NTs were captured, more than 30 au from the Sun and possibly as far out as 40 au near the formation region of the CCs (Nesvorný et al. 2020).

In this work we expand on the previous work available on the visible colours of NTs, with observations of 18 objects, 15 of which are new, which increases the number of NTs with known visible colours to 31.

## 2 OBSERVATIONS

We obtained optical $g$, $r$/R, and $i$/I photometry of 18 NTs with the Hale 5.1 m telescope (P200 hereafter) at Palomar Observatory, the Gemini North 8.1 m telescope (Gemini N hereafter), and the Keck I 10 m telescope at Mauna Kea Observatory, and the Gemini South 8.1 m telescope (Gemini S hereafter) at Cerro Pachón. Observations of our 18 NT targets were divided between the P200, Keck I, Gemini N, and Gemini S during 2020 – 2022. Five NTs were observed with the P200 using the Wafer-Scale Imager for Prime focus (WaSP) instrument (Nikzad et al. 2017). Three NTs were observed with Gemini N using the Gemini-North Multi-Object Spectrograph (GMOS-N) (Hook et al. 2004). Six NTs were observed with Gemini S using the Gemini-South Multi-Object Spectrograph (GMOS-S) (Gimeno et al. 2016) Four NTs were observed with Keck I using the Low Resolution Imaging Spectrometer (LRIS) (Oke et al. 1995). NTs on orbits which have been demonstrated with numerical calculations to be likely temporary captures from the background trans-Neptunian population were not observed (Horner & Lykawka 2012; Lin et al. 2021).

Photometry of NTs was obtained with Sloan Digital Sky Survey (SDSS)-equivalent $g$, $r$, and $i$ filters (Fukugita et al. 1996) with the P200, Gemini N, and Gemini S. Observations of NTs with Keck I used the SDSS-equivalent $g$ filter and the, Cousins R and I filters (Cousins 1976). Images were obtained in alternating $g$, $r$/R, and $i$/I sequences to minimize the effect on colour measurements caused by variations in the brightness of the NTs due to their rotation. Exposure times ranged between 30 and 300 s depending on conditions and the faintness of targets and the number of exposures per filter ranged between 3 and 15. The NTs were tracked at their non-sidereal rates, typically $\approx 0.05'' \, s^{-1}$. A complete technical description of the facility and instrumental set for our NT observations is provided in (Bolin et al. 2023).

Observations of NTs at all four sites occurred when the targets were as close to opposition as possible at at minimum airmass for maximum throughput and image quality. Seeing varied between 0.8 and 1.3″ as measured in the WaSP images taken with the P200, between 0.8 and 1.1″ as measured in the LRIS images taken with Keck I, was $\approx$0.5″ as measured in GMOS-N images taken with Gemini N, and varied between 0.6 and 0.9″ as measured in GMOS-S images taken with Gemini S. Standard stars from the Panoramic Survey Telescope and Rapid Response System survey (Pan-STARRS Tonry et al. 2012) were identified in the same fields as the science observations. A complete list of our observations can be found in Supplementary Table S1 of Bolin et al. (2023).

Taking a similar approach as Bolin et al. (2020a, 2020b, 2021, 2022), data from each facility were detrended and flattened using bias frames and flat-field images obtained with an inside-dome flat field panel. Cosmic rays and other blemishes were removed from individual images using the L.A. Cosmic Laplacian cosmic ray identification algorithm (van Dokkum 2001). The data were stacked in each photometric filter to enhance the signal of the NT detections. A complete description of the data reduction for each facility and instrument combination is available in the Supplemental Material (Bolin et al. 2023), along with Supplementary Fig. S1 showing examples of the P200, Gemini N/S, and Keck I NT detections.

The photometry of our NT targets and standard stars was performed using an aperture centred on the NT detections with a radius of 1.0 – 2.5″ that was 1.5 – 2 times the seeing measured in the images. Sky subtraction was completed by taking the median pixel value within an annulus centred on the NT detection that had an inner radius of 3.0 – 7.5″ and an outer radius of 6 – 11″. The NT photometry obtained with the P200, Keck I, and Gemini N/S was calibrated using the Pan-STARRS photometric catalogue (Tonry et al. 2012; Chambers et al. 2016) and transformed to SDSS and Johnson-Cousins passbands as approriate (Jordi et al. 2006).

## 3 RESULTS

The photometric measurements of our 18 NT targets are summarized in Table 1. We have plotted the optical colours of the NTs observed by us and by Sheppard & Trujillo (2006); Sheppard (2012); Jewitt (2018) and Lin et al. (2019) in $g - i$ versus $g - r$ colour space in Fig. 1. The average $g - i$ value of the 18 NTs is $\approx$0.84, equivalent to a spectral gradient of 8% / 100 nm normalized to 550 nm and significantly redder than the Sun which has $g - i = 0.58$ (Haberreiter et al. 2017; Willmer 2018). Out of the 18 NTs that we observed, four have $g - i$ colours $\gtrsim$1.2, the rough boundary separating the R and VR groups (Sheppard 2012): 2013 $VX_{30}$, 2011 $HM_{102}$, 2013 $TZ_{187}$, 2015 $VV_{165}$. Our measurements of the optical colours of the VR NT 2013 $VX_{30}$ with $g - i = 1.15 \pm 0.17$ is broadly consistent with the $g - i \approx 1.5$ by Lin et al. (2019), though their $g - i$ colour measurement more robustly places it past the 1.2 $g - i$ VR colour boundary.

One of the NTs we observed, 2011 $HM_{102}$, has $g - r = 0.91 \pm 0.07$ and $r - i = 0.34 \pm 0.06$ placing it into the VR category with $g - i = 1.25 \pm 0.06$. Parker et al. (2013) observed 2011 $HM_{102}$ and found $r - i = 0.31 \pm 0.04$, consistent with our measurements, but found $g - r = 0.51 \pm 0.04$, significantly bluer than our measured $g - r = 0.91 \pm 0.07$. The difference could be due to underestimated

**Table 1.** Photometry.

| Name | $m_r^1$ (mag) | $g-r$ (mag) | $r-i$ (mag) | $g-i$ (mag) | $S^2$ (% / 100 nm) |
|---|---|---|---|---|---|
| 2013 $VX_{30}$ | $23.06 \pm 0.1$ | $0.83 \pm 0.19$ | $0.32 \pm 0.11$ | $1.15 \pm 0.17$ | $20.14 \pm 13.18$ |
| 2012 $UD_{185}$ | $22.28 \pm 0.05$ | $0.60 \pm 0.11$ | $0.17 \pm 0.06$ | $0.77 \pm 0.09$ | $6.40 \pm 6.32$ |
| 2014 $QO_{441}$ | $23.35 \pm 0.04$ | $0.51 \pm 0.08$ | $0.33 \pm 0.06$ | $0.84 \pm 0.08$ | $9.14 \pm 6.09$ |
| 2012 $UV_{177}$ | $23.01 \pm 0.05$ | $0.74 \pm 0.07$ | $0.32 \pm 0.07$ | $1.06 \pm 0.08$ | $16.9 \pm 5.92$ |
| 2015 $VX_{165}$ | $24.15 \pm 0.10$ | $0.42 \pm 0.15$ | $0.22 \pm 0.11$ | $0.64 \pm 0.12$ | $1.85 \pm 8.16$ |
| 2011 $HM_{102}$ | $21.89 \pm 0.05$ | $0.91 \pm 0.07$ | $0.34 \pm 0.06$ | $1.25 \pm 0.06$ | $23.90 \pm 4.21$ |
| 2008 $LC_{18}$ | $23.06 \pm 0.05$ | $0.67 \pm 0.08$ | $0.21 \pm 0.07$ | $0.88 \pm 0.08$ | $10.34 \pm 5.79$ |
| 2013 $TZ_{187}$ | $23.09 \pm 0.04$ | $0.81 \pm 0.09$ | $0.38 \pm 0.05$ | $1.19 \pm 0.08$ | $21.79 \pm 6.40$ |
| 2014 $UU_{240}$ | $22.79 \pm 0.04$ | $0.45 \pm 0.07$ | $0.07 \pm 0.06$ | $0.52 \pm 0.07$ | $-2.05 \pm 4.74$ |
| 2015 $VW_{165}$ | $23.02 \pm 0.04$ | $0.38 \pm 0.07$ | $0.21 \pm 0.05$ | $0.59 \pm 0.06$ | $0.15 \pm 4.05$ |
| 2014 $RO_{74}$ | $24.01 \pm 0.10$ | $0.38 \pm 0.13$ | $0.26 \pm 0.15$ | $0.64 \pm 0.1$ | $1.78 \pm 9.09$ |
| 2014 $SC_{374}$ | $24.05 \pm 0.07$ | $0.44 \pm 0.09$ | $0.29 \pm 0.11$ | $0.73 \pm 0.1$ | $4.98 \pm 6.98$ |
| 2013 $RL_{124}$ | $23.76 \pm 0.09$ | $0.44 \pm 0.12$ | $0.34 \pm 0.14$ | $0.78 \pm 0.14$ | $6.55 \pm 9.52$ |
| 2015 $VV_{165}$ | $23.51 \pm 0.08$ | $0.93 \pm 0.11$ | $0.46 \pm 0.11$ | $1.39 \pm 0.12$ | $29.68 \pm 9.05$ |
| 2014 $YB_{92}$ | $23.44 \pm 0.06$ | $0.42 \pm 0.08$ | $0.15 \pm 0.09$ | $0.57 \pm 0.09$ | $-0.66 \pm 5.92$ |
| 2013 $TK_{227}$ | $23.79 \pm 0.06$ | $0.63 \pm 0.08$ | $0.38 \pm 0.12$ | $1.01 \pm 0.12$ | $14.67 \pm 9.01$ |
| 2013 $RC_{158}$ | $23.54 \pm 0.07$ | $0.32 \pm 0.09$ | $0.27 \pm 0.08$ | $0.59 \pm 0.08$ | $0.25 \pm 5.34$ |
| 2015 $VU_{207}$ | $21.98 \pm 0.04$ | $0.58 \pm 0.07$ | $0.09 \pm 0.05$ | $0.67 \pm 0.07$ | $2.66 \pm 4.61$ |
| Solar colours[3] | | $0.46 \pm 0.01$ | $0.12 \pm 0.01$ | $0.58 \pm 0.01$ | |

**Notes.** (1) Apparent *r*-band magnitude, (2) spectral gradient using the *g* and *i* measurements normalized to 550 nm, and (3) from Haberreiter et al. (2017) and Willmer (2018).

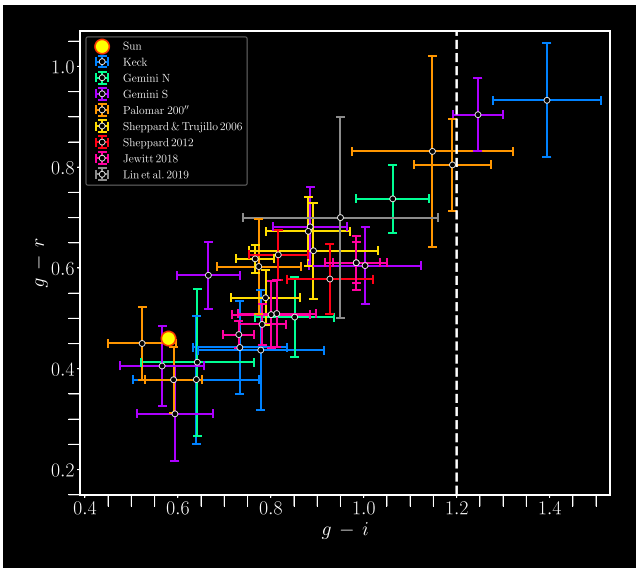


**Figure 1.** Sloan *g*, *r*, and *i* colours for the NTs observe in this work. Sloan NT colours from Sheppard & Trujillo (2006); Sheppard (2012); Jewitt (2018); and Lin et al. (2019) are also plotted. The vertical-dashed line at $g-i=1.2$ indicates the rough dividing line between the R and VR colour groups.The colours of the sun are plotted at $g-i=0.58$ and $g-r=0.46$ (Haberreiter et al. 2017; Willmer 2018).

uncertainties in the $g-r$ colour measurement by ourselves or by Parker et al. (2013), or due to light-curve variations. The SNR of our composite 2011 $HM_{102}$ *g* and *r* observations was ∼20 each and is consistent with the SNR expected from integration time calculations simulating the conditions of our observations.[1] To test the latter hypothesis, we measured the *g* magnitude of 2011 $HM_{102}$ in the *g* images taken at Gemini S taken in the *g*, *r*, and *i* sequence on 2022 July 18 UTC and found that there were no significant variations in the brightness of 2011 $HM_{102}$ in excess of ≈0.05 over the roughly half-hour observing sequence. In addition, our $g-i$ measurements of 2014 $QO_{441}$ of $g-i=0.84\pm0.08$ and of 2014 $UU_{240}$ of $g-i=0.52\pm0.07$ are generally consistent with the values measured by Lin et al. (2019).

[1] https://www.gemini.edu/instrumentation/gmos/exposure-time-estimation

## 4 DISCUSSION AND CONCLUSION

An initial impression of the NT colours in Fig. 1 is an apparent lack of a bimodal colour distribution. Following the example of Jewitt (2018), we have compared the $g-i$ colours of NTs with those of other dynamical classes. Using the optical colours compiled by the Minor Bodies in the Outer Solar system (MBOSS) data base (Hainaut et al. 2012), we have plotted the cumulative $g-i$ colour distribution of the Jovian Trojans (JTs), Centaurs, Scattered Disc objects, Plutinos, Resonant objects, HCs, CCs, and Detached Objects (Gladman et al. 2008) with the colours of NTs in Fig. 2. By visual inspection, the cumulative $g-i$ distribution of the JTs is distinct in lacking any VR objects compared to objects of the other TNO dynamical classes. However, it must be noted that while they lack VR objects, the Jupiter Trojans are bimodal in colour, albeit with bluer mean colours compared to the TNO population (e.g. Wong, Brown & Emery 2014; Wong & Brown 2015). The cumulative distribution of the $g-i$ colours of the NTs is located between these two groups, containing more VR objects than JTs, but disproportionately fewer VR objects compared to the other TNO classes, especially the CCs.

To quantify the differences between the $g-i$ distribution of the NTs and the $g-i$ distribution of other dynamical classes, we apply the Kolmogorov–Smirnov (KS) test which measures the maximum difference between two cumulative distributions (Darling 1957). The KS method tests the null hypothesis that two cumulative distributions are drawn from the same parent distribution. We have also applied the Kuiper variant of the KS test which is more sensitive to differences between distributions at their edges (Kuiper 1960). Table 2 shows the associated statistical score and p-value of the KS and Kuiper tests between the NTs and other TNO dynamical classes. The statistical

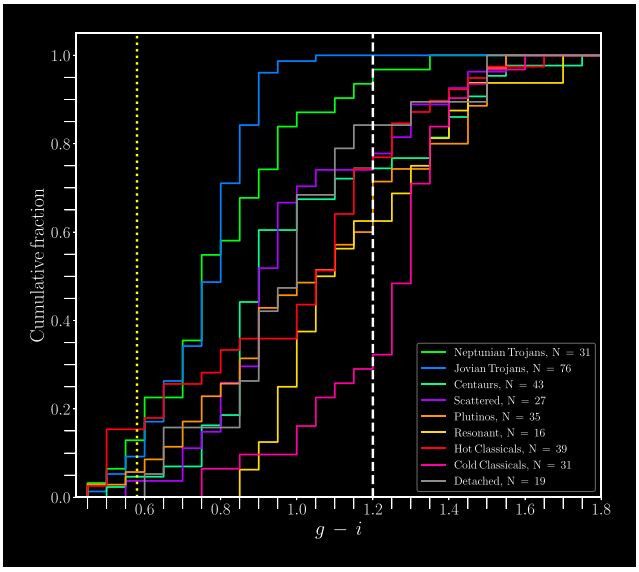


**Figure 2.** Cumulative distribution of the $g - i$ colours for the NTs and the $g - i$ colours for Jupiter Trojans, Centaurs, Scattered Disc Objects, Plutinos, Resonant objects, HCs, CCs, and Detached objects taken from Hainaut et al. (2012). The white vertical-dashed line at $g - i = 1.2$ indicates the rough division line between R and VR objects. The yellow vertical-dotted line indicates the colour of the Sun at $g - i = 0.58$ (Haberreiter et al. 2017; Willmer 2018).

**Table 2.** Kolmogorov–Smirnov (KS) and Kuiper (K) variant NT statistical score and p-values (P).

| Class | N | KS score | KS P | K score | K P |
|---|---|---|---|---|---|
| NTs | 31 | 0.0 | 1.0 | 0.0 | 1.0 |
| JTs | 76 | 0.2186 | 0.2138 | 0.2830 | 0.0882 |
| Centaur | 43 | 0.4449 | 0.0010 | 0.3946 | 0.0012 |
| Scattered disc | 27 | 0.4182 | 0.0086 | 0.4053 | 0.0008 |
| Plutinos | 35 | 0.4203 | 0.0039 | 0.4389 | <0.0001 |
| Resonant | 16 | 0.7137 | <0.0001 | 0.6992 | <0.0001 |
| HCs | 39 | 0.4797 | 0.0004 | 0.5833 | <0.0001 |
| CCs | 31 | 0.7419 | <0.0001 | 0.7419 | <0.0001 |
| Detached objects | 19 | 0.5195 | 0.0019 | 0.4873 | <0.0001 |

score is a quantified measure of the maximum difference between two cumulative distributions with a larger statistical score corresponding to a lower p-value for data sets of similar size. The comparison between the NTs and the CCs results in the largest statistical score of 0.74 for both the KS and Kuiper test corresponding to a p-value of $< 0.0001$. The comparison between the NTs and JTs results in the smallest statistical score of 0.22 corresponding to a p-value of 0.2138 for the KS test and a statistical score of 0.28 and a p-value of 0.0882 for the Kuiper test. The KS and Kuiper tests between the NTs and the Centaurs, Scattered Disc objects, Plutinos, Resonant objects, HCs, and Detached objects have p-values <0.005.

The $g - i$ colour distribution of the NTs is distinct compared to other TNO classes. Previous studies show a much larger p-value for the tests between the cumulative optical colour distribution of the NTs and JTs (Jewitt 2018). Our expanded sample with additional VR NTs implies dissimilarity in the $g - i$ colours of NTs and JTs, although it only rules out the null hypothesis at the $1 - 2\sigma$ level with a p-value of ≈0.08 – 0.21. The small number of the VR NTs and the large error bars on the $g - i$ colours may make drawing a strong conclusion about the differences between the optical colours of NTs and JTs difficult.

TNO evolutionary models predict that the observed proportion of VR and R objects in different TNO classes is a result of the separation between VR and R objects in the original TND located at a radial distance from the Sun denoted as $r_*$ (Nesvorný et al. 2020). The combined sample of our observed NTs with those from the literature results in a VR to R ratio of ≈ 1:8. Although the location of $r_*$ may also be affected by the density profile of the original TND, a higher proportion of VR objects to R objects may imply a closer in value of $r_*$ compared to a lower proportion. In the case of a disc with an exponential density profile, an NT VR to R ratio of 1:8 may imply a $r_*$ interior to 35 au, whereas a truncated profile may imply a $r_*$ interior to 30 au. In either case, the discovery of additional NTs and measurements of their optical colours will provide additional constraints on the compositional gradient of the original TND. In addition to the location of the transition boundary between R and VR objects in the original TBD, the colours of TNOs could also be affected by post-formation evolutionary effects such as collisions and thermal processing (McKinnon et al. 2008). Additional obsevations of NTs are forthcoming in Markwardt et al. 2023, in revision).

## ACKNOWLEDGEMENTS

We thank the referee for their helpful comments that improved the quality of this manuscript. The authors appreciate the help from O. Oberdorf with the reduction of GMOS-N and GMOS-S images. CF acknowledges support from the Heising-Simons Foundation (grant number 2018-0907). We wish to recognize and acknowledge the cultural role and reverence that the summit of Mauna Kea has always had within the indigenous Hawaiian community. The authors wish to recognize and acknowledge the cultural significance that Palomar Mountain has for the Pauma Band of the Luiseño Indians. Based on observations obtained at the international Gemini Observatory, a program of NSF's NOIRLab, which is managed by the Association of Universities for Research in Astronomy (AURA) under a cooperative agreement with the National Science Foundation on behalf of the Gemini Observatory partnership. Some of the data presented herein were obtained at the W. M. Keck Observatory, which is operated as a scientific partnership among the California Institute of Technology, the University of California and the National Aeronautics and Space Administration.

## 5 DATA AVAILABILITY

The data underlying this article will be shared on reasonable request to the corresponding author.

## REFERENCES

Bernardinelli P. H. et al., 2022, ApJS, 258, 41
Bolin B. T. et al., 2021, AJ, 161, 116
Bolin B. T. et al., 2023, Supplemental Material
Bolin B. T. et al., 2020a, AJ, 160, 26
Bolin B. T. et al., 2020b, ApJ, 900, L45
Bolin B. T. et al., 2022, MNRAS, 517, 49
Brown P. et al., 2011, Meteoritics and Planetary Science, 46, 339
Chambers K. C. et al., 2016, preprint (arXiv:1612.05560)
Cousins A. W. J., 1976, MNRAS, 81, 25
Darling D. A., 1957, The Annals of Mathematical Statistics, 28, 823
DeMeo F. E., Carry B., 2014, Nature, 505, 629
Fukugita M., Ichikawa T., Gunn J. E., Doi M., Shimasaku K., Schneider D. P., 1996, AJ, 111, 1748

Gimeno G. et al., 2016, in Evans C. J., Simard L., Takami H., eds, Society of Photo-Optical Instrumentation Engineers (SPIE) Conference Series Vol. 9908, Ground-based and Airborne Instrumentation for Astronomy VI. p. 99082S
Gladman B., Marsden B. G., Vanlaerhoven C., 2008, in Barucci M. A., Boehnhardt H., Cruikshank D. P., Morbidelli A., Dotson R., eds, The Solar system Beyond Neptune. p. 43
Gomes R., Nesvorný D., 2016, A&A, 592, 146
Haberreiter M., Schöll M., Dudok de Wit T., Kretzschmar M., Misios S., Tourpali K., Schmutz W., 2017, Journal of Geophysical Research (Space Physics), 122, 5910
Hainaut O. R., Boehnhardt H., Protopapa S., 2012, A&A, 546, 115
Hook I. M., Jørgensen I., Allington-Smith J. R., Davies R. L., Metcalfe N., Murowinski R. G., Crampton D., 2004, PASP, 116, 425
Horner J., Lykawka P. S., 2012, MNRAS, 426, 159
Jewitt D., 2018, AJ, 155, 56
Jordi K., Grebel E. K., Ammon K., 2006, A&A, 460, 339
Kuiper N. H., 1960, Proceedings of the Koninklijke Nederlandse Akademie van Wetenschappen, Series A., 63, 38
Lin H. W. et al., 2019, Icarus, 334, 79
Lin H. W. et al., 2021, Icarus, 361, 114391
Markwardt L. et al., 2023, in revision
McKinnon W. B., Prialnik D., Stern S. A., Coradini A., 2008, in Barucci M. A., Boehnhardt H., Cruikshank D. P., Morbidelli A., Dotson R., eds, The Solar system Beyond Neptune. p. 213
Morbidelli A., Emel'yanenko V. V., Levison H. F., 2004, MNRAS, 355, 935
Morbidelli A., Nesvorný D., 2020, in Prialnik D., Barucci M. A., Young L., eds, The Trans-Neptunian Solar system. p. 25
Nesvorný D. et al., 2020, AJ, 160, 46
Nikzad S. et al., 2017, Journal of Astronomical Telescopes, Instruments, and Systems, 3, 036002
Oke J. B. et al., 1995, PASP, 107, 375
Parker A. H. et al., 2013, AJ, 145, 96
Schwamb M. E. et al., 2019, ApJS, 243, 12
Sheppard S. S., 2012, AJ, 144, 169
Sheppard S. S., Trujillo C. A., 2006, Science, 313, 511
Tonry J. L. et al., 2012, ApJ, 750, L99
Trujillo C. A., Brown M. E., 2002, ApJ, 566, L125
van Dokkum P. G., 2001, PASP, 113, 1420
Williams J. P., Cieza L. A., 2011, ARA&A, 49, 67
Willmer C. N. A., 2018, ApJS, 236, 47
Wong I., Brown M. E., 2015, AJ, 150, 174
Wong I., Brown M. E., 2016, AJ, 152, 90
Wong I., Brown M. E., 2017, AJ, 153, 145
Wong I., Brown M. E., Emery J. P., 2014, AJ, 148, 112

## SUPPORTING INFORMATION

Supplementary data are available at *MNRASL* online.

**suppl_data**

Please note: Oxford University Press is not responsible for the content or functionality of any supporting materials supplied by the authors. Any queries (other than missing material) should be directed to the corresponding author for the article.

This paper has been typeset from a TEX/LATEX file prepared by the author.